Three sub-events composing the 2011 off the Pacific coast of Tohoku Earthquake (M_w 9.0) inferred from rupture imaging by back-projecting teleseismic *P* waves

Hao Zhang, Zengxi Ge, and Luyuan Ding

Department of Geophysics, School of Earth and Space Sciences, Peking University, Beijing 100871, China

(Received April 4, 2011; Revised June 9, 2011; Accepted June 11, 2011; Online published September 27, 2011)

High-quality vertical component seismograms of teleseismic *P* waves recorded at 151 stations of the European seismic network have been used to image the rupture process of the 2011 Tohoku Earthquake rapidly by a two-step back-projection method. The spatio-temporal distribution of rupture fronts suggests that the earthquake ruptured northeastwards and southwestwards over a total length of more than 340 km during at least 143 s. The fact that three fault segments ruptured at regions having different lateral heterogeneities implies that the earthquake comprised three sub-events. The first sub-event ruptured northeastwards during the first 25 s, and then turned to the northwest direction. The second sub-event ruptured at a relatively high speed of 2.78∼4.70 km/s. The third sub-event ruptured with a direction variation from southwest to southeast near the latitude of 37°. In addition, considering that the first front of the second sub-event appeared at 74.6 s and was about 28 km away from the epicenter, we propose that the second sub-event might have been triggered by the localized increase in tectonic stress in the vicinity of the hypocenter that resulted from the rupture of the first sub-event.

Key words: The 2011 Tohoku Earthquake, rupture imaging, back projection.

1. Introduction

On March 11, 2011, the magnitude 9.0 Tohoku Earthquake struck off the northeast coast of Honshu, Japan (UTC 05:46:23, hypocenter 38.322°N, 142.369°E, 32 km depth (U.S. Geological Survey (USGS), http://earthquake.usgs.gov/earthquakes/eqinthenews/2011/usc0001xgp/)). The disastrous earthquake and the accompanying powerful tsunami led to tens of thousands of deaths and many missing. This disaster emphasizes the importance of rapidly and accurately imaging the rupture process for post-earthquake emergency response and tsunami warnings.

In recent years, the back-projection method has been used as an effective approach to image the spatio-temporal rupture process (Ishii *et al*., 2005; Krüger and Ohrnberger, 2005; Walker *et al*., 2005). The only prior parameter used in this method is the location of the hypocenter, which was determined in almost real-time by the USGS. Meanwhile, the calculations of the back-projection method are so straightforward that it takes no more than half an hour to effectively image the rupture process. To image the two-dimensional spatial rupture process of the 2011 Tohoku Earthquake, we apply here a two-step back-projection method (Zhang and Ge, 2010) to process the broadband teleseismic *P* waves that were recorded by 151 seismic stations of the European seismic network, referred to as "the Euro network".

doi:10.5047/eps.2011.06.021

2. Data

We downloaded teleseismic *P*-wave data of the 2011 Tohoku Earthquake recorded by 344 European stations from the website (http://www.orfeus-eu.org/cgi-bin/wilberII/wilber_page1.pl) of the Observations and Research Facilities for European Seismology (ORFEUS). Considering the epicentral distance and azimuth coverage of stations, as well as the quality of their data, 151 broadband seismograms from the stations were selected as shown in Fig. 1(a). The reference station (ZAG in Fig. 1(a)), with the shortest distance to the center (47.654°N, 14.912°E) of the Euro network, is about 82.5° away from the epicenter and has an azimuthal angle of ∼325°. The orientation of the Euro network to the epicenter is nearly perpendicular to the strike direction (193°, presented by USGS). This orientation, together with the large aperture, of the Euro network is of great utility in resolving the rupture along the strike direction.

Teleseismic *P* waves over a period of time of 220 s were used to isolate the *P* wave from other phases, such as *PP*. To save calculation time, only vertical component seismograms were considered; i.e. only the reference (ZAG) and 24 other traces shown in Fig. 1(b). Considering the coherence and resolution of the data, seismograms with a sample rate of 20 Hz were high-pass filtered with a cut-off frequency of 0.2 Hz, at which the array response function (Rost and Thomas, 2002; Xu *et al*., 2009) was calculated to illuminate the array geometry and azimuth on the spatial resolution (Fig. 1(c)).

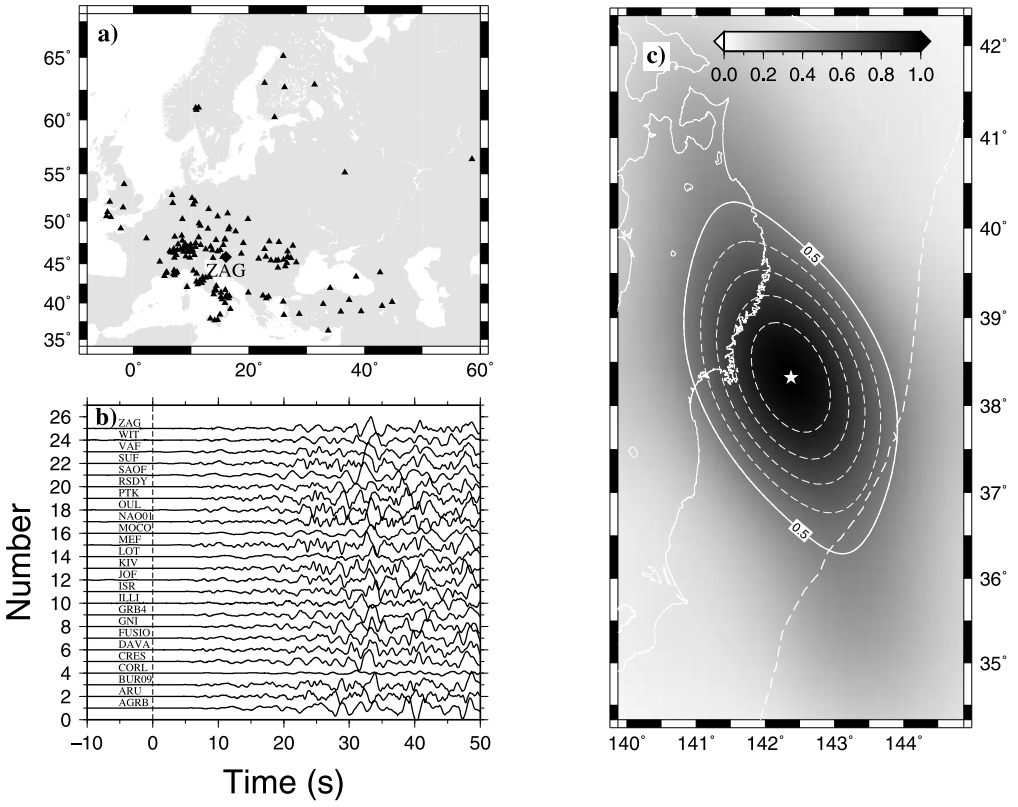

Fig. 1. Features related to the stations of the Euro network. (a) Distribution of 151 stations (black triangles and a black diamond) throughout Europe that compose the Euro network. The large black diamond with the label "ZAG" indicates the reference station. (b) Examples of the vertical-component high-quality normalized seismograms from 25 stations with a time length of 60 s, which are high-pass filtered with a cut-off frequency of 0.2 Hz. (c) The array response function of the Euro network to the source region at 0.2 Hz. The black star indicates the epicenter of the Tohoku Earthquake. The dashed line depicts the Japan trench. The contour lines indicate the normalized beam energy with a interval of 0.1.

3. Methodology

This study employed the two-step back-projection method described by Zhang and Ge (2010). In the first step, *P* waves were back-projected to find locations of the rupture fronts at the apparent rupture times. Then, rupture times of the fronts were derived from their own locations and apparent rupture times.

To identify the rupture fronts of the 2011 Tohoku Earthquake, the source region (34.32∼42.32°N, 139.87∼144.87°E) was spatially gridded into blocks of $0.1^\circ \times 0.1^\circ$. This process resulted in 4131 grid points referring to potential rupture fronts. Due to the small dip of the fault plane (14°, given by USGS), the potential rupture fronts were fixed at a depth (Ishii *et al.*, 2007) of 32 km, the hypocenter depth given by USGS. The theoretical travel time was calculated in 1-D Earth velocity model AK135 (Kennett *et al.*, 1995) for each pair of potential rupture front and station. However, due to lateral heterogeneities along ray paths, there is always a small difference between theoretical and real travel times (Fig. 1(b)). Therefore, the theoretical travel times from the stations to the hypocenter were calibrated by aligning the initial 30 s of the teleseismic *P* waves through cross-correlation. These time calibrations of the hypocenter were applied to other potential fronts (Xu *et al.*, 2009).

4. Results and Analyses

This process of the back-projection approach made it possible to obtain an image of the rupture process. The image was used to generate the normalized energy and rupture time relationships of the rupture fronts as shown in Fig. 2(b). The rupture ending time was determined as 143 s due to the sudden decrease in the energy released (Fig. 2(b)). To mitigate the smearing of the fronts in time, rupture fronts located at the same place for several continuous time steps were removed except one with the maximum releasing energy. The image of the rupture process was obtained as shown in Fig. 2(a). The rupture time-distance relationship (Fig. 2(c)) shows that there were high-frequency energy-radiation peaks located at 14 km northeast, 34 km southwest and 191 km southwest of the epicenter, corresponding to rupture times of 23 s, 77 s, and 111 s, respectively. Moreover, the time-distance relationship shows that in the first 74 s the earthquake ruptured northeastwards over a length of 92 km at an average rupture speed of 0.92∼1.10 km/s, while no rupture fronts appeared on the southwest branch. Due to non-uniquely determining the time corresponding to the main contributing wave energy within the 30-s window length, there is an uncertainty in the estimation of the rupture velocity (Krüger and Ohrnberger, 2005). The first rupture front on the southwest branch started at 74.6 s at a distance of ∼28 km away from the epicenter. The earthquake continued to rupture southwestwards over 150 km at an average speed of 2.78∼4.70

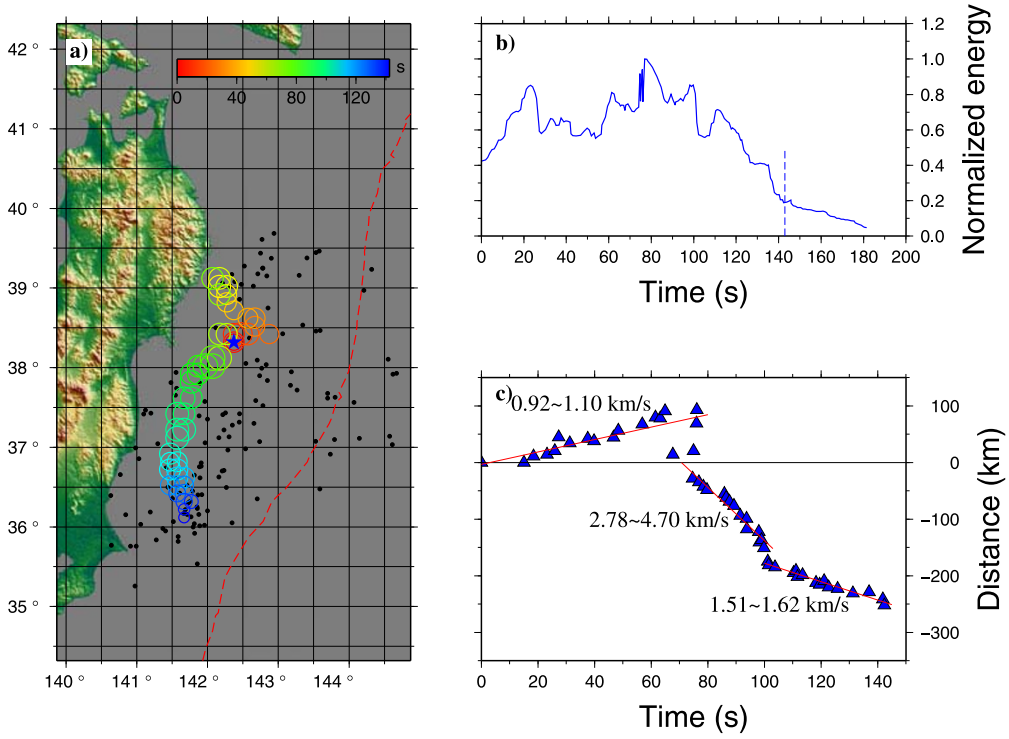

Fig. 2. Rupture imaging of the 2011 Tohoku Earthquake. (a) Spatial and temporal (color bar shows the rupture time) distribution of three high-frequency energy sources during the whole rupture time of at least 143 s (given in Fig. 2(b)). First, the earthquake ruptured towards the northeast and then northwest of the epicenter. After a time delay, the rupture started from the epicenter again and extended towards the southwest with a distinct variation of the rupture direction at the latitude of 37°. (b) The relationship between released energy and rupture time. The dashed blue line indicates the ending time of the earthquake (143 s). There are three energy-radiation peaks at 23, 77, and 111 s. (c) The rupture time-distance relationship during the rupture process. First, the earthquake ruptured towards the northeast and then northwest of the epicenter at a slow rate of 0.92∼1.10 km/s. The rupture front did not appear on the southwestern branch until 74 s. Then the earthquake ruptured towards the southwest for 150 km at an average rate of 2.78∼4.70 km/s from about 74 s to 100 s. Finally, the earthquake ruptured to the southeast for a length of about 110 km on the third fault segment at an average rate of 1.51∼1.62 km/s.

km/s until 100 s, when the rupture velocity suddenly decreased to 1.51∼1.62 km/s. The rupture continued for an additional 110 km at this lower velocity and finally ended at 143 s. The rupture features described above imply that the Tohoku Earthquake consisted of three stages. Because the time lag between the first and second stages was about 74 s, we propose that the second stage might have been triggered by the first stage due to the localized increasing tectonic stress focused in the vicinity of the hypocenter, as a result of the rupture of the first stage. In addition, there were three other prominent phenomenon observed during the rupture process. First, the rupture front propagated at a very slow velocity along the strike direction during the first 25 s (Fig. 2(c)) with a very large energy-radiation peak northeast of the epicenter at 23 s (Fig. 2(b)). Second, the rupture direction of the first stage turned from northeast to northwest near the latitude of 38.5° at about 23 s (Fig. 2(a)). Third, there was a spatial gap of about 20 km during no more than 2 s and a distinct directional variation near the latitude of 37.0°, which separated the second stage from the third.

5. Discussion

The rupture evolution of an earthquake can be affected by the fault-zone properties (Di Stefano *et al.*, 2011). In this study, most of the rupture features observed from the back-projection imaging (Fig. 2(a)) can also be associated with the lateral heterogeneities of the *P*- and *S*-wave velocity and Poisson's ratio (PR) structures which have been well investigated by tomographic imaging (Zhao *et al.*, 1992, 2007) on the slab boundary. There are two kinds of wave velocity and PR anomalies in the rupture zone. One is characterized by high *P* and *S* velocity and low PR anomaly, which implies a more rigid medium. The other has a low *P* and *S* velocity and high PR anomaly, which implies a more ductile medium. The hypocenter occurred in a region at a latitude of 38.32°, which is near the boundaries of high and low velocity and PR. The rupture extended northeastwards after the initiating earthquake. An energy peak was radiated when the rupture went through the boundary of velocity and PR anomalies into a more ductile region near 85.5° at 23 s. Due to the northwest-elongated anomalies distribution of the region, the rupture of the northern branch turned to the northwest direction. Next, the earthquake ruptured southwestwards. The second energy peak was released when the rupture went through a boundary of velocity and PR anomalies into a rigid region near the latitude of 38.0° at 77.0 s. Since the region of 37.0°∼38.0° is more rigid, the rupture extended at a high rate across this region. Then the rupture arrived at an anomaly boundary near the latitude of 37.0° at 110 s, when the energy peak of the third stage was radiated. Since the rupture zone of the third stage with a latitude below 37° has a southeast elongation of low *P* and *S* wave and high PR anomalies, the rupture direction turned to the

southeast direction at a low rupture velocity. Therefore, due to the lateral heterogeneities of the *P* and *S* velocity and PR on the slab boundary of the northeast Japan arc, the rupture process of the 2011 Tohoku Earthquake consisted of three sub-events having different rupture velocities and energy-radiation peaks.

Not long after the earthquake, many source inversions of other types of data, such as tsunami, and broadband teleseismic data, were carried out to investigate the slip of the earthquake (Lay *et al*., 2011a, b). However, the areas of the large slip in these source models are quite different from most of the back-projection results (Koper *et al*., 2011). We think the main reason for the apparent inconsistency is that the main frequency of data used by back-projection is much higher than other types of data adopted by source inversions. The rupture features of the 2011 Tohoku Earthquake derived from back-projection have come from small-scale rupture structures. In contrast, the slip models from inversions are optimal solutions of the entire rupture process, in which small-scale features are smoothed. In addition, the characteristic frequency of the radiated signal varies during the rupture for a large earthquake (Kiser and Ishii, 2011). Thus, source models inverted from different types of data with different frequency bandwidths reflect the rupture features of different stages and scales of the 2011 Tohoku Earthquake.

6. Conclusions

In this paper, a two-step back-projection method, an array technique based on a non-plane-wave assumption, was applied to image the rupture process of the 2011 M_w 9.0 Tohoku Earthquake. The rupture imaging resulting from this study shows that the 2011 Tohoku Earthquake has a total rupture length of over 340 km and duration of at least 143 s, and ruptures to the northeast first and then to the southwest. Three energy radiation peaks occurred at 23 s, 77 s, and 110 s, which correspond to 14 km northeast, 28 km southwest, and 191 km southwest of the epicenter, respectively. According to analyses of the lateral heterogeneities of *P*- and *S*-wave velocities in the rupture zone, the 2011 Tohoku Earthquake consists of three sub-events. The first one ruptured northeastwards and then northwards over ∼90 km during the first 74 s at a speed of 0.92∼1.10 km/s. Then the second one ruptured southwestwards from 74 s to 100 s with a length of over 150 km at a relatively high speed of 2.78∼4.70 km/s, and might have been triggered by the increasing tectonic stress focused in the vicinity of the hypocenter as a result of the rupture of the first sub-event. The third one ruptured about 110 km southeastwards at an average speed of 1.51∼1.62 km/s until the rupture ended at 143 s.

Some interesting rupture details of our model are presented here. The first sub-event ruptured around the epicenter during the first 25 s after the initiating earthquake. The second sub-event ruptured at a relatively high velocity on the megathrust fault. A sudden rupture-velocity variation appeared between the second and third sub-events on the southwest branch near the latitude of 37°. Most of the rupture details are closely related to lateral heterogeneities of the *P* and *S* velocity and PR structures on the slab boundary of the northeast Japan arc. Although some details need further confirmation, we can say that the rupture imaging infers that the 2011 Tohoku Earthquake comprised three sub-events (the first one on the northeast, and the last two on the southwest).

Acknowledgments. We thank Dr. J. Y. Ning, Z. K. Shen, and Mr. K. Tao for their advice, and two anonymous referees for the constructive reviews of this manuscript. We also thank P. Wessel and Walter H. F. Smith (1991) for their GMT software, and ORFEUS for the data downloaded from the website of ORFEUS. This paper is supported by the national sciences foundation of China (grant Nos. 41074029, 40821160552 and 40821062). This work was done when one of the authors (Z. Ge) is visiting the University of California, Santa Cruz. The support for this visit from China Scholarship Council and UCSC are appreciated.

References

Di Stefano, R., C. Chiarabba, L. Chiaraluce, M. Cocco, P. De Gori, D. Piccinini, and L. Valoroso, Fault zone properties affecting the rupture evolution of the 2009 (Mw 6.1) L'Aquila earthquake (central Italy): Insights from seismic tomography, *Geophys. Res. Lett*., **38**, doi:10.1029/2011GL047365, 2011.

Ishii, M., P. M. Shearer, H. Houston, and J. E. Vidale, Extent, duration and speed of the 2004 Sumatra-Andaman earthquake imaged by the Hi-Net array, *Nature*, **435**, 933–936, 2005.

Ishii, M., P. M. Shearer, H. Houston, and J. E. Vidale, Teleseismic P wave imaging of the 26 December 2004 Sumatra-Andaman and 28 March 2005 sumatra earthquake ruptures using the hi-net array, *J. Geophys. Res*., **112**, B11307, doi:10.1029/2006JB004700, 2007.

Kennett, B. L. N., E. R. Engdahl, and R. Buland, Constraints on seismic velocities in the earth from travel times, *Geophys. J. Int*., **122**, 108–124, 1995.

Kiser, E. and M. Ishii, The 2010 Mw 8.8 Chile earthquake: Triggering on multiple segments and frequency-dependent rupture behavior, *Geophys. Res. Lett*., **38**, doi:10.1029/2011GL047140, 2011.

Koper, K. D., A. R. Hutko, T. Lay, C. J. Ammon, and H. Kanamori, Frequency-dependent rupture process of the 2011 M_w 9.0 Tohoku Earthquake: Comparison of short-period *P* wave backprojection images and broadband seismic rupture models, *Earth Planets Space*, **63**, this issue, 599–602, 2011.

Krüger, F. and M. Ohrnberger, Tracing the rupture of the M_w = 9.3 Sumatra earthquake over 1,150 km at teleseismic distance, *Nature*, **435**, 937–939, 2005.

Lay, T., C. J. Ammon, H. Kanamori, L. Xue, and M. J. Kim, Possible large near-trench slip during the 2011 M_w 9.0 off the Pacific coast of Tohoku Earthquake, *Earth Planets Space*, **63**, this issue, 687–692, 2011a.

Lay, T., Y. Yamazaki, C. J. Ammon, K. F. Cheung, and H. Kanamori, The 2011 M_w 9.0 off the Pacific coast of Tohoku Earthquake: Comparison of deep-water tsunami signals with finite-fault rupture model predictions, *Earth Planets Space*, **63**, this issue, 797–801, 2011b.

Rost, S. and C. Thomas, Array seismology: Methods and applications, *Rev. Geophys*., **40**(3), 1008, doi:10.1029/2000RG000100, 2002.

Walker, K. T., M. Ishii, and P. M. Shearer, Rupture details of the 28 March 2005 Sumatra M_w 8.6 earthquake imaged with teleseismic P waves, *Geophys. Res. Lett*., **32**, L24303, doi:10.1029/2005GL024395, 2005.

Wessel, P. and W. Smith, Free software helps map and display data, *Eos. Trans. AGU*, **72**, 441, 1991.

Xu, Y., K. D. Koper, O. Sufri, L. Zhu, and A. R. Hutko, Rupture imaging of the M_w 7.9 12 May 2008 Wenchuan earthquake from back projection of teleseismic P waves, *Geochem. Geophys. Geosyst*., **10**(4), 1–17, doi:10.1029/2008GC002335, 2009.

Zhang, H. and Z. X. Ge, Tracking the rupture of the 2008 Wenchuan earthquake by using the relative back-projection method, *Bull. Seismol. Soc. Am*., **100**(5B), 2551–5560, doi:10.1785/0120090243, 2010.

Zhao, D., A. Hasegawa, and S. Horiuchi, Tomographic imaging of P and S wave velocity structure beneath northeastern Japan, *J. Geophys. Res*., **97**, 19,909–19,928, 1992.

Zhao, D., Z. Wang, N. Umino, and A. Hasegawa, Tomographic imaging outside a seismic network: Application to the northeast Japan arc, *Bull. Seismol. Soc. Am*., **97**, 1121–1132, 2007.

H. Zhang, Z. Ge (e-mail: zge@pku.edu.cn), and L. Ding